Supporting Information

Electron Beam Facilitated Structural Evolution of Nano-Zinc-Oxide

Siyu Liu[1#], Rui Wang[1#], Xiang Cai[2], Yanming Wang[3*]*

[1.] School of Mechanical Engineering, Shanghai Jiao Tong University, Shanghai, 200240, China.

[2.] University of Michigan - Shanghai Jiao Tong University Joint Institute, Shanghai Jiao Tong University, Shanghai, 200240, China.

[3.] The Global Institute of Future Technology, Shanghai Jiao Tong University, Shanghai, 200240, China.

[*]Corresponding author: E-mail: liusiyu@sjtu.edu.cn , yanming.wang@sjtu.edu.cn

Table of contents

SI1. Experimental methods

ZnO crystals, referred to as 'monomers' in this study, were synthesized using the pulsed laser method, consistent with previous reports[1]. The precursor solution was produced by dissolving 1.5 mM zinc acetate dihydrate ($Zn(CH_3COO)_2 \cdot 2H_2O$) in 25 mL of deionized water and mixing with 25 mL of ethanol (all reagents obtained from Sigma-Aldrich)[2], and with 1 mL of dilute aqueous ammonia (pH ≈ 10) added dropwise with continuous vigorous stirring at room temperature. Si (100) wafers cut into 1 cm × 1 cm pieces were cleaned with deionized water and immersed in the precursor solution. A copper TEM grid (400 mesh, coated with a 15–30 nm silicon monoxide support film; SF400-Cu, Electron Microscopy Sciences, Hatfield, PA) was positioned film-side-up on the silicon substrate, and its edges were sealed with copper tape to ensure stability during irradiation.

Laser irradiation was performed for 1 s using a ytterbium pulsed fiber laser (wavelength 1064 nm, pulse width 100 ns, repetition rate 100 kHz) at a power density of 1.27 kW cm^{-2}. The short period of irradiation triggered hydrothermal reactions that produced ZnO nanocrystals and intermediate species, referred to as monomers in this study, directly on the grid surface. Following laser treatment, the grid was removed, rinsed with deionized water, air-dried, and subjected to argon plasma cleaning for 40 s prior to microscopy. Transmission electron microscopy was carried out using an FEI TALOS F200X instrument equipped with a 200 kV field emission gun. Images and

videos were acquired with a bottom-mounted Gatan US1000 2K × 2K CCD camera, with video recording at a frame rate of approximately 30 frames per second.

SI2. Vacancy formation and subsequent evolution under e-beam irradiation

An in-situ observation of e-beam-induced crystal evolution was shown in Figure S1. Crystalline membranes were thinned and introduced with defects after a few minutes of exposure to the e-beam. Hexagonal pores formed, expanded, and eventually created voids that led to the tearing of the membranes. It could be observed that the atoms moves under the irradiation of the e-beam, and from the FFT diffraction pattern, we could observe that the crystallinity various with time.

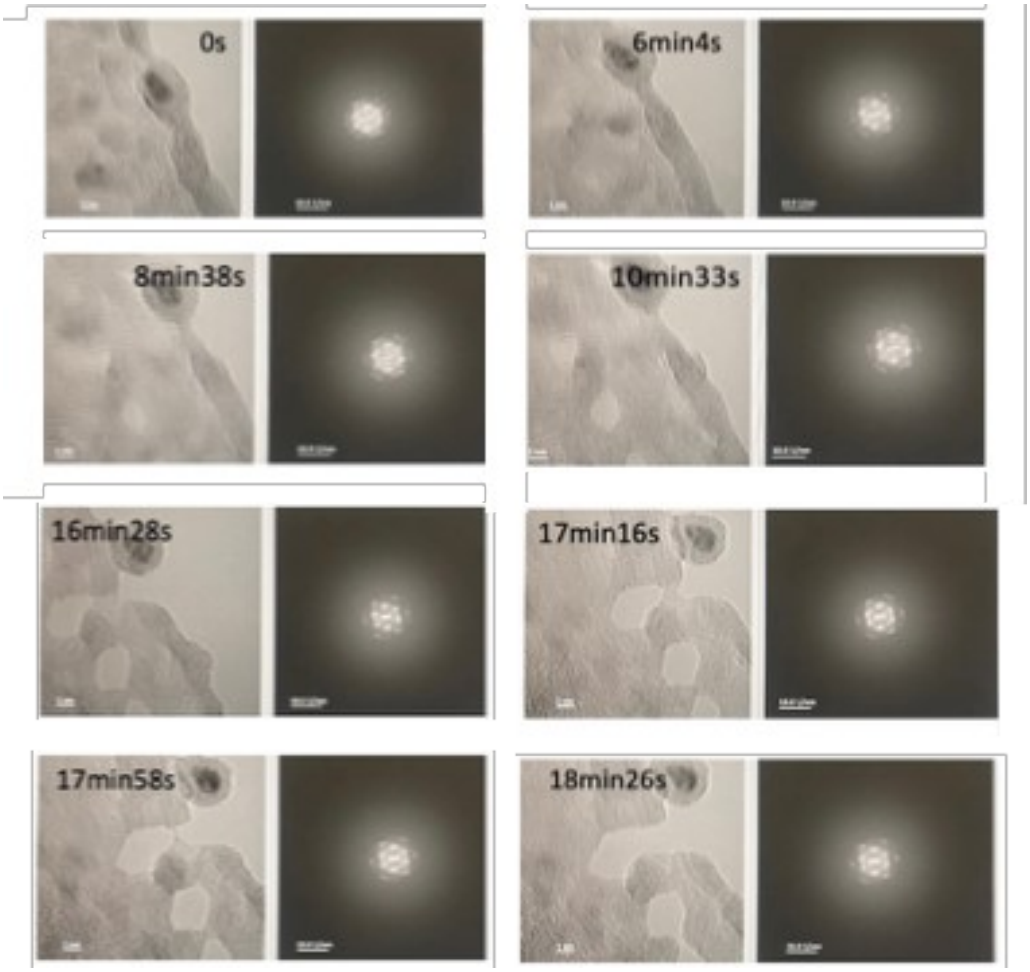

Figure S1 ZnO crystal with a thin film structure evolution under the irradiation of e-beam. *In situ* TEM snapshots at representative times with corresponding FFT patterns.

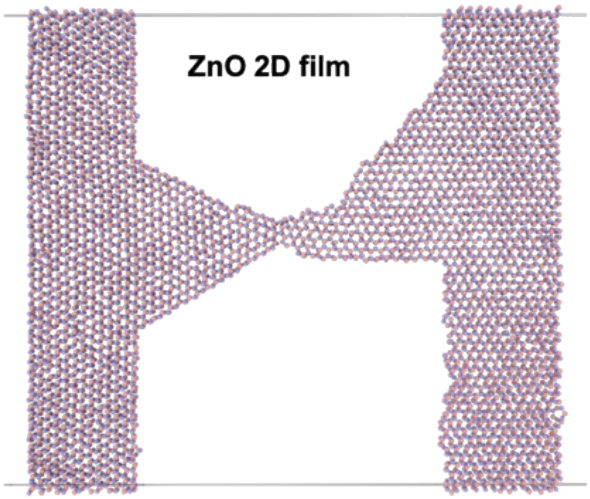

Figure S2 The initial configuration of H-shaped ZnO 2D film [0001] with grain boundary in MD simulation.(Snapshot in top view.) Red balls were O atoms. Blue balls were Zn atoms.

In the simulation of 2D ZnO-film with grain boundary, in order to keep the charge neutrality, we removed one Zn atom and one O atom in each case under irradiation. In irradiation-on-Area A-cases, one atom was removed from the boundary area while another removed from the stable area. In irradiation-on-Area B-cases, two atoms were both removed from the stable area.

SI3. Details of DFT calculations

All density functional theory (DFT) calculations were performed by VASP (Vienna ad initio simulation package) [1-3]. Spin unrestricted generalized-gradient approximation (GGA) with the Perdew-Burke-Ernzerhof functional (PBE) [4] were adopted. The first Brillouin zone was sampled with a 5×5×1 k-mesh. Figure S3a presented the bulk ZnO after relaxation. For Figure S3b, the ZnO structure was cleaved along [0001] to create a 2D structure. There was a vacuum region with thickness of 15 Å in the 2D structure to avoid the interaction between the periodic structure. Also, the top three layers in 2D structure were set to be moved freely. Compared with Figure S3a, the shape of ZnO in Figure S3b became a flatter honeycomb-like configuration after relaxation. The trend was more obvious in upper layer. All the results demonstrate that the MD calculation was reasonable.

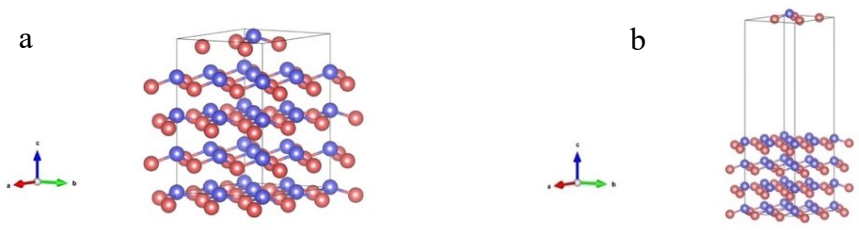

Figure S3. (a) bulk ZnO structure (after relaxation) (b) 2D honeycomb-like ZnO structure(after relaxation). Red balls were O atoms. Blue balls were Zn atoms.

SI4. Mass transfer through surface diffusion

An evolution of a cluster of crystals in 2 mins are shown in Figure S4, which are snapshotted from Movie S2. The mass diffusion within a cluster of crystals leads to crystal rearrangement, as could be obviously tracked through particles at the edges.

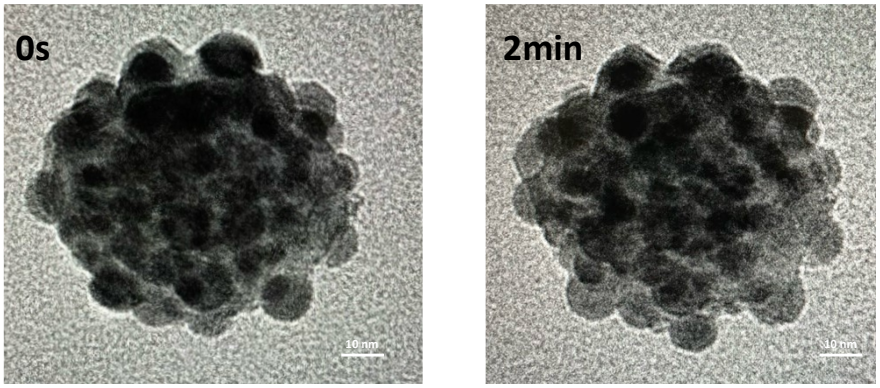

Figure S4. Mass transfer among connected ZnO particles within a cluster by diffusion.

SI5. Hypothesis test of morphologies of ZnO particles in Figure 3

In Figure 3, it is observed that particle A lacks faceting and lattice fringes, while particles B and C exhibit hexagonal shapes with clear fringes, we infer distinct structural differences. Moreover, since no other particles were observed in the system, we assume the process follows mass conservation: the mass gained by particles B and C corresponds to the mass lost by particle A.

Here, we evaluate statisticallly the hypothesis that particle A behaves as a thin film (mass $\propto$ area), while particles B and C (and their aggregate B+C) behave as spheres (mass $\propto$ area$^{3/2}$), using BIC (Bayesian Information Criterion).[5,6]

Model M1 assumes particle A is a thin film, with its mass proportional to its projected area ($m_A \propto S_A$), while particles B and C (or their aggregate B+C) are spheres with mass proportional to area$^{3/2}$. Thus, changes in spherical volume proxies (ΔV_{target}) should be linearly related to changes in A's area (ΔS_A). By contrast, Model M0 assumes particle A is also a sphere, so the predictor is A's volume proxy ($\Delta V_A = \Delta(S_A^{3/2})$). Comparing these models allows testing whether A behaves more like a thin film or a sphere under mass-conserving transfer. The results are shown in Table S1 and Figure S5.

Before aggregation ($t < 23$), both the thin-film model (M1: Δ(Vb+Vc) vs ΔSa) and the sphere model (M0: Δ(Vb+Vc) vs ΔVa) fit the data poorly, with positive slopes and very low R^2 values. This suggests that prior to aggregation, the system does not exhibit a clean two-pool exchange, possibly due to parallel processes or noise.

Table S1. BIC comparison table

Segment	Model	BIC

Pre (< 23 s)	M1 (A=thin film, B+C spheres)	536.51
Pre (< 23 s)	M0 (A=sphere, B+C spheres)	536.52
Post (≥ 23 s)	M1 (A=thin film, B+C spheres)	609.64
Post (≥ 23 s)	M0 (A=sphere, B+C spheres)	610.07

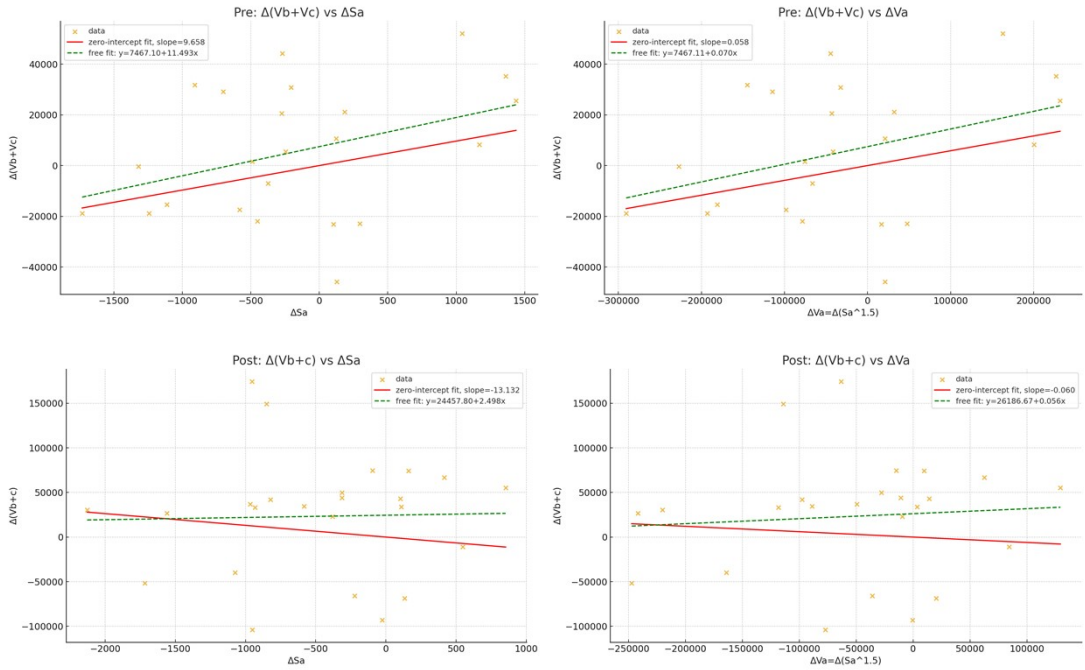

Figure S5. Fitting curves (ΔV vs ΔSa and ΔVa, before and after aggregation, with zero- and free-intercept fits)

After aggregation (t ≥ 23 s), the thin-film model produces a negative slope as expected (A shrinks while B+C grows). Although the fit remains noisy, the direction of the effect is consistent with the hypothesized geometry. BIC values are slightly lower for the thin-film model in both segments, with ΔBIC < 2, which counts as weak but consistent evidence favoring the thin-film hypothesis. Mass conservation diagnostics further support this view: the composite total mass proxy was flatter and more stable after the merge than before, consistent with a cleaner two-reservoir transfer mechanism.

In summary, the post-aggregation evidence aligns with the hypothesis that A behaves like a thin film while B and C (or their aggregate B+C) behave as spheres under mass-conserving conditions. Before aggregation, the signal is less clear, but no evidence contradicts the hypothesis.

SI6. Simulation details of di-nanoparticles-system

During the simulation of di-nanoparticles-system under electron irradiation, we identified the vaporization and deposition events in four kinds with different transfer paths of atoms: atoms from crystal particle to crystal particle, atoms from crystal particle to amorphous particle, atom from amorphous particle to amorphous particle and atoms from amorphous particle to crystal particle. The counts of different events occurred during the simulation was shown in Figure S6.

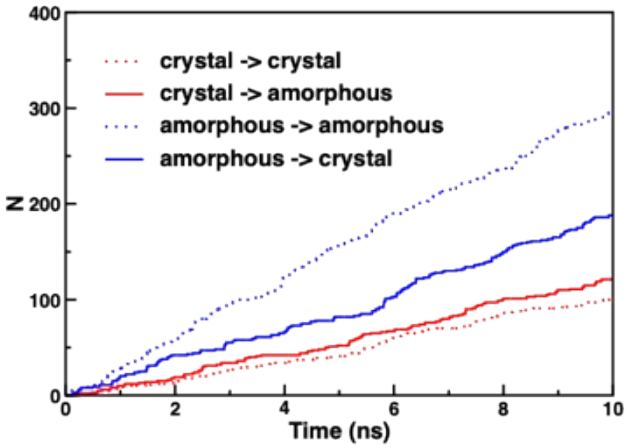

Figure S6 Events with different mass transfer paths occurred during the simulation of di-nanoparticles-system as a function with time(cumulated).

With the local vibration induced by electron irradiation, the whole system first became unstable. And then during more and more atoms vapored to deposit on the crystal particle, the crystal particle was grown gradually with time, leading to more stable system. The difference of potential energy with initial structure showed this crystallization process in Figure S7, compared with no-irradiation simulation. Obviously, the initial amorphous-crystal system is thermodynamically stable at room temperature. The crystallization cannot happen without the mass-transfer induced by irradiation. It also indicated the mass transition process leading to a lower potential energy.

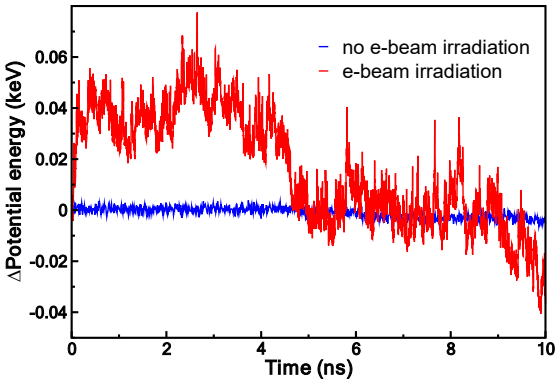

Figure S7 The evolution of the system potential energy. The red line was the system under e-beam irradiation. The blue line was the system without e-beam irradiation.

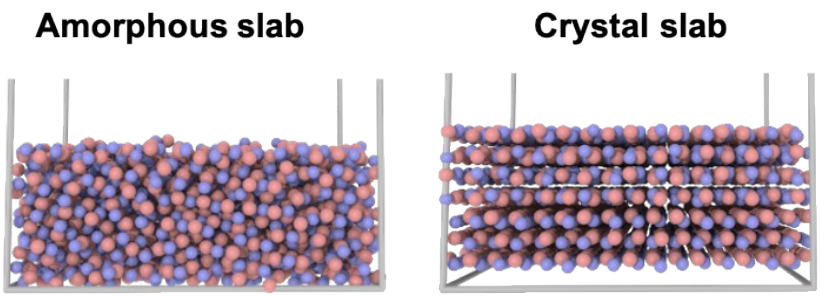

Figure S8 The initial amorphous ZnO slab and crystal ZnO slab configurations with periodic boundaries parallel to the surface. There were a 20 Å thick vacuum above the slab surface. Red balls were O atoms. Blue balls were Zn atoms.

In our simulation, the average potential energy of the crystal and amorphous slab-surface was -7.34 and -6.75 eV/atom, respectively, indicating that the amorphous slab surface was more unstable. Moreover, in the initial structure of our di-particle system, there were 1024 atoms in cyrstal particle and 1980 atoms in amorphous particle. The average potential energy of the crystal particle and the amorphous particle was -7.37 and -7.32 eV/atom, respectively. The potential energy difference of each atom from the average value of the particle was shown with population and total numbers in Figure S9. It suggested that there were more unstable atoms in amorphous particle, which leading to more veporization from the amorphous particle.

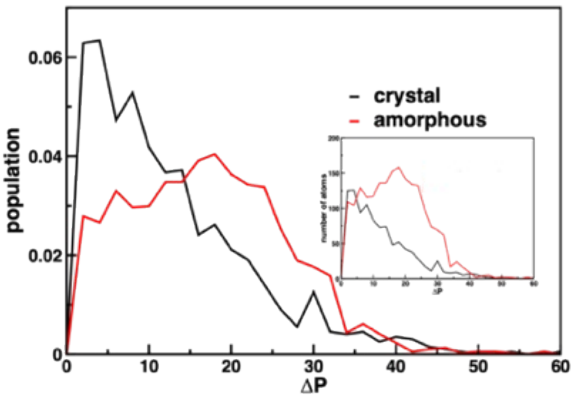

Figure S9 The distribution of the potential energy difference of atoms in the crystal and amorphous particle, respectively.

SI7. In-situ TEM data list: Movie S1-S3

MOVIE S1

In-situ observation of e-beam-induced evolution of 2D ZnO crystals during breakage. Corresponding snapshots are presented in Figure 1 of the main text.

MOVIE S2

The mass diffusion within a cluster of crystals leads to crystal rearrangement. Snapshots from the beginning and end of the video are shown in Figure S4, highlighting significant size changes in the particles, particularly those at the edges. This is likely due to mass diffusion between the particles.

MOVIE S3

In-situ observation of a mass transfer process between two disconnected particles. Corresponding snapshots are presented in Figure 3a of the main text.

References

(1) Kresse, G.; Hafner, J. Ab initio molecular-dynamics simulation of the liquid-metal-amorphous-semiconductor transition in germanium. *Phys Rev B Condens Matter* **1994**, *49* (20), 14251-14269.

(2) Kresse, G.; Furthmüller, J. Efficient iterative schemes for ab initio total-energy calculations using a plane-wave basis set. *Physical Review B* **1996**, *54* (16), 11169-11186.

(3) Perdew, J. P.; Burke, K.; Ernzerhof, M. Generalized Gradient Approximation Made Simple. *Physical Review Letters* **1996**, *77* (18), 3865-3868.

(4) Kresse, G.; Furthmüller, J. Efficiency of ab-initio total energy calculations for metals and semiconductors using a plane-wave basis set. *Computational Materials Science* **1996**, *6* (1), 15-50.

(5) Schwarz, G. Estimating the dimension of a model. *Annals of Statistics,* **1978,** 6(2), 461–464.

(6) Kass, R. E., & Raftery, A. E. Bayes factors. *Journal of the American Statistical Association*, **1995,** 90(430), 773–795.